AGU PUBLICATIONS

Geochemistry, Geophysics, Geosystems

RESEARCH ARTICLE
10.1002/2015GC005845

Special Section:
The Lithosphere-asthenosphere System

Lithospheric architecture beneath Hudson Bay

Robert W. Porritt[1], Meghan S. Miller[1], and Fiona A. Darbyshire[2]

[1]Department of Earth Sciences, University of Southern California, Los Angeles, California, USA, [2]Centre de recherche GEOTOP, Université du Québec à Montréal, Montréal, Quebec, Canada

Abstract Hudson Bay overlies some of the thickest Precambrian lithosphere on Earth, whose internal structures contain important clues to the earliest workings of plate formation. The terminal collision, the Trans-Hudson Orogen, brought together the Western Churchill craton to the northwest and the Superior craton to the southeast. These two Archean cratons along with the Paleo-Proterozoic Trans-Hudson internides, form the core of the North American craton. We use S to P converted wave imaging and absolute shear velocity information from a joint inversion of P to S receiver functions, new ambient noise derived phase velocities, and teleseismic phase velocities to investigate this region and determine both the thickness of the lithosphere and the presence of internal discontinuities. The lithosphere under central Hudson Bay approaches ~350 km thick but is thinner (~200–250 km) around the periphery of the Bay. Furthermore, the amplitude of the LAB conversion from the S receiver functions is unusually large for a craton, suggesting a large thermal contrast across the LAB, which we interpret as direct evidence of the thermal insulation effect of continents on the asthenosphere. Within the lithosphere, midlithospheric discontinuities, significantly shallower than the base of the lithosphere, are often imaged, suggesting the mechanisms that form these layers are common. Lacking time-history information, we infer that these discontinuities reflect reactivation of formation structures during deformation of the craton.

Key Points:
- The thick lithosphere of Hudson Bay has significant structural variation
- We directly image the thermal blanketing on the asthenosphere
- The lithospheric thickness of Hudson Bay is 200–350 km

Supporting Information:
- Supporting Information S1
- Software S1

Correspondence to:
R. W. Porritt,
rporritt@usc.edu

Citation:
Porritt, R. W., M. S. Miller, and F. A. Darbyshire (2015), Lithospheric architecture beneath Hudson Bay, *Geochem. Geophys. Geosyst.*, *16*, 2262–2275, doi:10.1002/2015GC005845.

Received 6 APR 2015
Accepted 7 JUN 2015
Accepted article online 11 JUN 2015
Published online 14 JUL 2015

1. Introduction

The formation and preservation of cratonic lithosphere is a fundamental problem in Earth science; it requires neutrally buoyant and relatively cold rocks to exist at depths of up to ~350 km maintained, with little deformation, since the Archean. A solution to this is the isopynic hypothesis of *Jordan* [1988] where the negative thermal density of cold material is offset by positive chemical buoyancy from a melt-depleted composition of cratonic mantle. Processes whereby this thick lithosphere may have been formed in the warmer Archean mantle can be broadly characterized as either vertical processes, such as plume impingement, or lateral tectonic processes such as stacking of oceanic plates or differentiation in arc magmas [e.g., *Lee*, 2006; *Aulbach*, 2012]. The analyses of mantle xenoliths presented in *Lee* [2006] and *Aulbach* [2012] have shown support for both end-member processes, but it is likely that a mixture of processes was active during craton formation. Constraining the degree to which each process has influenced cratonization has important ramifications for understanding the dynamics of the early Earth.

Recent advances in seismic imaging techniques and seismograph station coverage have led to the identification of a midlithospheric discontinuity (MLD) in many cratonic settings [e.g., *Abt et al.*, 2010; *Ford et al.*, 2010]. This feature is usually characterized as a negative conversion in receiver functions at depths of ~80–120 km, a depth range corresponding to relatively high shear velocity inferred from 1-D surface wave inversions [e.g., *Abt et al.*, 2010; *Darbyshire and Eaton*, 2010; *Fischer et al.*, 2010; *Miller and Eaton*, 2010]. Thermal, mechanical, and chemical models for this discontinuity have been proposed and recently reviewed in *Selway et al.* [2015], but no primary mechanism has yet been determined. Thermo-chemical models suggest the MLD is a manifestation of a depleted upper cratonic mantle where the heat transport regime transitions from conductive to convective, but this transition may occur over such a large depth interval that it is unclear if a conversion would be identified with receiver functions. Alternatively, mechanical models suggest a variation in anisotropy reflecting the accretion or deformation history of lithospheric mantle [e.g., *Snyder et al.*, 2013; *Yuan and Romanowicz*, 2010]. Finally, pockets of partial melt could cause these negative impedance contrasts seen in the receiver functions, but they should also cause significant low shear velocity

zones and would imply significant weakness within the cratons and/or metasomatized mineral phases, which are not typically observed. These models of MLDs have implications for the formation of cratons and thus improved observations of the structure of these discontinuities may help further illuminate the formation history of the continents.

The core of the North American craton is located in the Hudson Bay region. Global shear velocity models from long period surface waves indicate high wavespeed material to depths greater than 250 km [e.g., *Gung et al*., 2003*; Lekic and Romanowicz*, 2011]. As a well-preserved craton, with Archean basement rocks exposed at the surface and an apparently thick lithosphere, it provides an important context for studying craton formation. If lateral tectonic processes dominated the formation we may expect to see dipping structural planes or variations in anisotropy consistent with major province boundaries. Alternatively, vertical processes may lead to deeper, more isolated conversions reflecting low-density residuum left following differentiation processes from plume head impingement. These two distinct processes will both leave structural variations within the lithosphere, which can be observed as MLDs. Furthermore, these features may provide zones of weakness along which further episodes of deformation localize.

It has been commonly thought that continental lithosphere may have an effect of thermally insulating the upper asthenosphere [e.g., *Grigné and Labrosse*, 2001; *Lenardic et al*., 2005]. This effect is inferred in the Canadian Shield from measurements of low ($\sim$30 mW/m^2) heat flux relative to the global continental average of $\sim$65 mW/m^2 [*Pollack et al*., 1993]. Combining these measurements with shear velocity information, *Lévy et al*. [2010] constrain the heat flux at the base of the lithosphere to $\sim$11 mW/m^2 in the Superior craton [see also *Rolandone et al*., 2003]. For comparison, estimates of mantle heat flow in the Kaapvaal craton are slightly higher, reaching $\sim$17 mW/m^2 [*Jaupart and Mareschal*, 1999]. This low heat flow value is consistent with insulation of the upper asthenosphere as it implies there is little asthenospheric heat loss into the upper boundary layer. Therefore, a thermally insulated upper asthenosphere should cause a significant wave-speed gradient between the base of the lithosphere and the top of the asthenosphere.

1.1. Tectonic Setting

Taking a large scale view, the Hudson Bay region is composed of two Archean proto-continents, the Western Churchill and Superior, which collided at $\sim$1.9–1.8 Ga in the Trans-Hudson Orogeny (THO). The Western Churchill can be further subdivided into the Rae and Hearne domains along the Snowbird Tectonic Zone (Figure 1). The Rae domain contains the oldest Sr and Nd model ages of the Churchill craton, reaching 3.6 Ga [*Peterson et al*., 2011]. Only a small portion of the Hearne domain is covered in the current study, but its southwestern limit potentially extends to the Wyoming Province in the northern United States [*Whitmeyer and Karlstrom*, 2007]. The Hearne is distinguishable by its isotopically juvenile Neoarchean volcanic rocks and lack of Archean activity younger than 2.66 Ga [*Davis et al*., 2004, 2006], and is overlain in parts by the Paleoproterozoic Wollaston Basin [*Whitmeyer and Karlstrom*, 2007]. The Superior craton can also be subdivided into several regions, with primarily east-west striking fabrics in the west and south, but more northwest-southeast striking subprovinces in the northeast [*Percival*, 2007], evident from magnetic anomalies (Figure 1). During the THO, the Superior craton collided with the southern and eastern promontories of the Western Churchill craton [*Gibb*, 1983; *Darbyshire and Eaton*, 2010; *Pawlak et al*., 2011]. This collision likely trapped smaller terranes in the Trans-Hudson orogenic belt in the center of modern Hudson Bay [*Eaton and Darbyshire*, 2010]. The southeastern border of the Superior craton is formed by the Grenville deformation front, which occurred over the period of 1.3 – 0.9 Ga [*Dalziel*, 1991; *Moores*, 1991; *Whitmeyer and Karlstrom*, 2007].

Recent studies using the Hudson Bay Lithospheric Experiment (HuBLE) data and other seismograph stations in the region and its surroundings have explored the seismic anisotropy [*Bastow et al*., 2011; *Darbyshire et al*., 2013; *Frederiksen et al*., 2007; *Darbyshire and Lebedev*, 2009; *Pawlak et al*., 2012; *Snyder et al*., 2013], isotropic wavespeed [*Darbyshire et al*., 2007, 2013; *Eaton and Darbyshire*, 2010; *Frederiksen et al*., 2007; *Pawlak et al*., 2011, 2012; *Bastow et al*., 2014], and discontinuity structure [*Darbyshire et al*., 2007; *Snyder et al*., 2013; *Thompson et al*., 2010, 2011] with various methods and a recent summary of these studies is presented in *Bastow et al*. [2014]. However, the lithosphere-asthenosphere boundary (LAB) in much of the region is poorly constrained due to the gradational nature of the boundary in cratons [e.g., *Abt et al*., 2010; *Fischer et al*., 2010]. The current estimate of the lithospheric thickness in the region comes from a regional surface wave tomography study, in which the LAB is defined as the 1.7% fast contour in shear velocity with respect

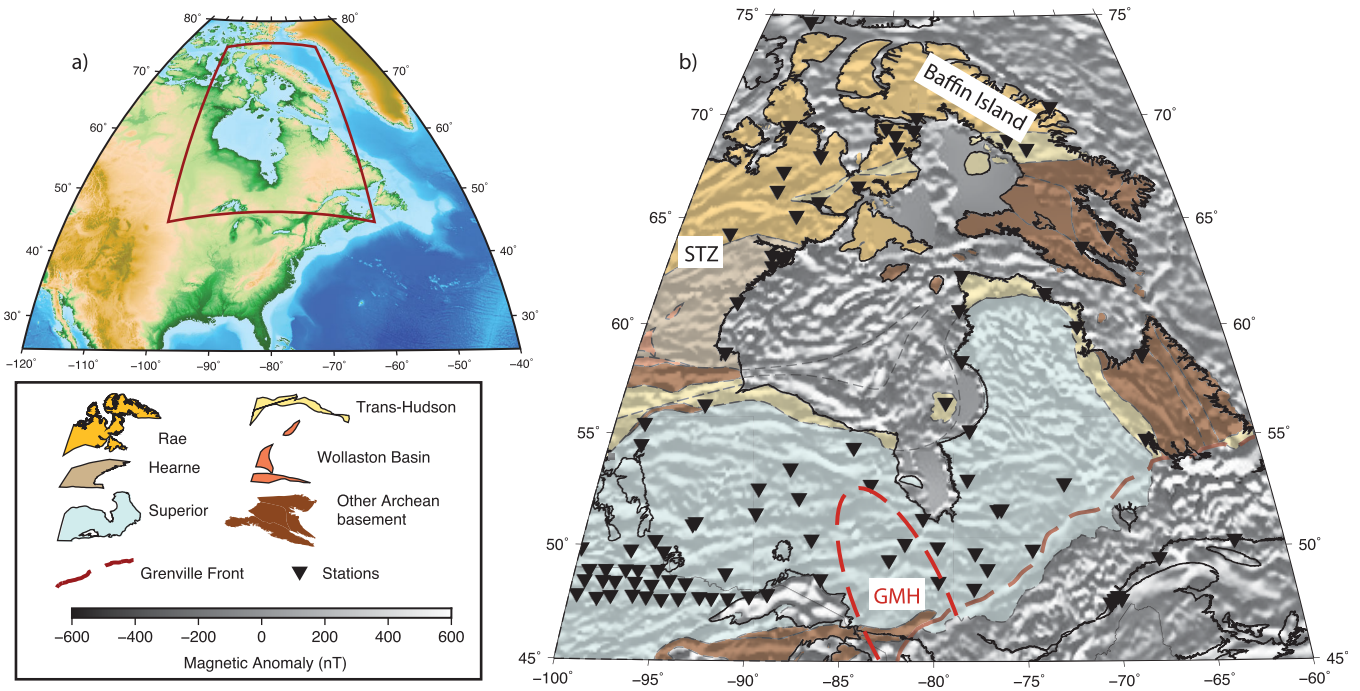

Figure 1. Location map of the study region. (a) Topographic map with red box indicating eastern Canada, centered on Hudson Bay. (b) Hudson Bay region and surroundings, with physiographic boundaries from *Whitmeyer and Karlstrom* [2007] overlain on magnetic anomalies. Stations shown are those used in the SdP CCP. STZ—Snowbird Tectonic Zone. GMH—Great Meteor Hotspot track.

to a global reference [*Darbyshire et al*., 2013]. However, the resolution of this study is limited to Hudson Bay itself and the peripheries due to the locations of crossing ray paths between stations. In this paper, we expand on previous observations with a new S to P receiver function (SRF) common conversion point stack (SdP CCP) for the region and its surroundings.

2. Structural Imaging

The discontinuity structure is investigated using data from ∼100 broadband seismograph stations deployed around the region (Figure 1). The majority of the stations near the Bay are from the POLARIS component of HuBLE deployed from 2004 to 2012, with the main data-acquisition phase being 2007–2009. The Canadian National Seismograph Network permanent stations also provide data and the University of Manitoba provides six additional stations. We further increase our data set by taking advantage of USArray stations in the southern segment of our study region. In order to ensure a broad sampling of ray paths, we choose an overall data time window for the following analysis from January 2000 through September 2014.

2.1. S to P Receiver Functions

The SRF method is able to image the discontinuity structure by mapping out converted P waves from incident S or SKS phases [*Vinnik*, 1977; *Kind et al*., 2012; *Yuan et al*., 2006]. SRFs are sensitive to impedance (density x velocity) contrasts along the ray path and are being increasingly used to image lithosphere scale structure [e.g., *Abt et al*., 2010; *Cooper and Miller*, 2014; *Foster et al*., 2013; *Hansen et al*., 2013; *Kind et al*., 2012; *Kumar et al*., 2012; *Lekic et al*., 2011; *Levander and Miller*, 2012; *Miller and Agostinetti*, 2011, 2012; *Miller and Eaton*, 2010; *O'Driscoll and Miller*, 2015; *Vinnik*, 1977; *Yuan et al*., 2006]. S to P receiver functions are often preferable to P to S receiver functions (PRF) for studying the LAB, as they are free of multiple crustal conversions, which often arrive at the same delay time as the LAB conversion in PRFs. We compute 7,992 SRFs and 3,125 SKS receiver functions (SKSRF, which utilize the incident SKS arrival rather than the direct S) in a ray-centric coordinate frame [*Vinnik*, 1977] with a water-level deconvolution [*Langston*, 1977] to isolate converted P phases from the incident SV arrival. The SRF are computed on arrivals at distances between 55° and 91° while the SKSRF use arrivals from 89° to 112° epicentral distance (see Figure 2 for a map of events used).

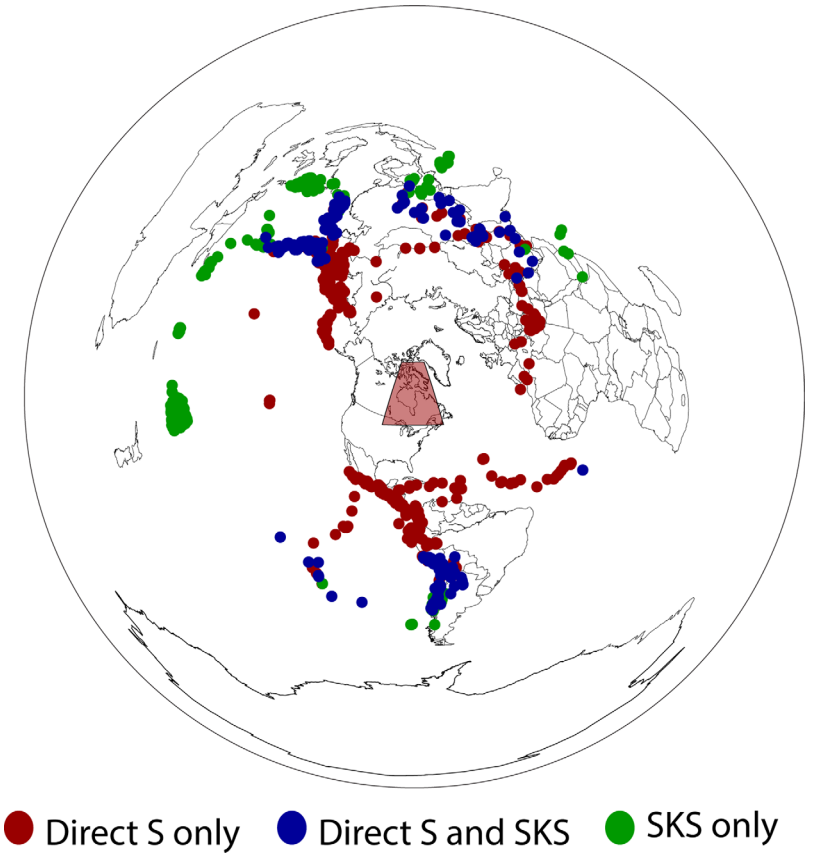

Figure 2. Events used in the SdP CCP stack.

2.2. Shear Velocity Model

Hudson Bay has been shown to have a significantly high seismic velocity lithospheric lid [e.g., *Darbyshire et al*., 2013] and we account for this when mapping the receiver functions from the time domain to depth by computing a mean shear velocity model through joint inversions of PRFs and surface wave phase velocities. The surface wave data were composed of teleseismically derived isotropic Rayleigh wave phase velocities [*Darbyshire et al*., 2013] between 20 and 220 s period and ambient noise tomography (ANT) derived phase velocities between 7 and 32 s period following the method of *Bensen et al*. [2007]. The teleseismic data of *Darbyshire et al*. [2013] use a two-station method for measuring phase velocity. 33 stations across the Hudson Bay region are used in the study, with an average of 15 events per interstation path. The path data are inverted for a set of phase velocity maps following the method outlined in *Deschamps et al*. [2008] and *Darbyshire and Lebedev* [2009]. The ANT data sre computed by correlations of seismic noise of up to 15 years (January 2000 to September 2014) of vertical component seismic data for ∼220 stations around the area including USArray stations in the southern Superior craton. The noise correlations are filtered between 5 and 150 s period, phase velocities are measured with a frequency-time analysis [e.g., *Dziewonski et al*., 1969; *Levshin et al*., 1989] between 7 and 32 s, and the path-wise correlations are quality controlled by requiring a minimum signal-to-noise ratio of 20 and minimum path length of 3 wavelengths. The paths are then inverted to calculate phase velocity maps using the method of *Barmin et al*. [2001]. Checkerboard tests for the ANT data indicate the best recovery is in the southern part of the study area where USArray stations provide a high spatial density of data coverage; however the mean phase velocity, necessary for the inversion, is well recovered everywhere (see the supporting information for a map of stations used, phase velocity maps, and resolution tests). In order to prepare for a joint inversion with PRFs, we linearly interpolate from the 2-D phase velocity maps to produce 1-D phase velocity curves at each station location.

New radial-over-vertical component PRFs are computed at ∼120 stations around the Hudson Bay region using the iterative deconvolution method [*Ligorria and Ammon*, 1999] for teleseismic P wave arrivals from

earthquakes greater than magnitude 5.5. This set of stations is similar to that used in the ANT analysis, but with ~100 of the USArray stations removed as they are well south of the focus of our study area (see the supporting information for a map of the stations used for PRFs). The PRFs are filtered with a Gaussian pulse width of 2.5, as is typical for crustal scale studies and trace edited in FuncLab [*Eagar and Fouch*, 2012] before being stacked into ray parameter and back-azimuth bins of 0.010 s/km by 45 degrees.

We implement the *joint96* program from Computer Programs in Seismology [*Herrmann*, 2013] to jointly invert the stacked PRFs and surface wave observations for shear velocity structure [e.g., *Bailey et al*., 2012; *Liu et al*., 2012]. This program begins with a linearized inversion based on a simple velocity model with a constant-velocity upper layer (4.48 km/s) from the surface to 55 km depth and a smoothly increasing velocity through the mantle beneath (see Figure 3 and the supporting information). The initial high-velocity upper layer is chosen to reduce the possibility of the inversion inserting artificial low velocity crustal layers [*Herrmann*, 2013] and the smooth velocity changes reduce the risk of a priori bias in Moho depth inference. The solver iterates through forward calculations of synthetic dispersion curves and receiver functions allowing the upper crust to vary up to 0.9 km/s per iteration and restricting the upper mantle variations to 0.1 km/s. The inversion uses a trade-off parameter to determine the relative weighting between the phase velocities and the receiver functions [*Julia et al*., 2000]. Adjusting this parameter has little effect on the final model or the reported model fits, which we attribute to the high consistency in the stacked PRFs and tomographically inferred phase velocities. The joint inversion shear velocity results are averaged at each depth to make a mean Hudson Bay shear velocity model (Figure 4), which we then use to map the SRFs and SKSRFs to depth and stack them into common conversion point bins of $2^\circ \times 2^\circ \times 10$ km from the surface to 400 km depth.

3. Results

3.1. Shear Velocity

We use a 3-D linear interpolation of the joint inversion shear velocity results to infer a 3-D model. This model is compared to the 3-D model of *Darbyshire et al*. [2013] derived from solely teleseismic Rayleigh wave phase velocities in Figure 5 to evaluate which 3-D model is more suitable for interpretation alongside the SdP CCP volume. Because both models use the same teleseismic phase velocities as inputs, they are not fully independent, but they do provide different estimates of the overall shear velocity structure. We observe relatively low velocities in the crust (~10–40 km depth) of the joint inversion model, as well as lower shear velocity throughout the lithosphere and higher asthenosphere velocity in the joint inversion relative to the surface wave only model. Inferring the LAB from the ~1.7% fast contour with either model yields similar results in the southernmost section, but the central section through Hudson Bay and the northern section through the Rae domain appear to give significantly thicker lithosphere in the surface wave only model of *Darbyshire et al*. [2013]. There are at least three probable causes for these differences: (1) the joint inversion is only defined at the stations while the surface wave model is defined between the stations, (2) the surface wave only model uses a Markov Chain Monte Carlo method rather than an iterative linearized method allowing a more complete search of the model space, along with a smooth spline-based parameterization throughout the upper mantle, and (3) the joint inversion forces more velocity perturbation shallower to create the necessary phase conversions and contains ANT derived phase velocity information at periods primarily sampling the crust. We infer that the *Darbyshire et al*. [2013] model is more reliable under the Bay where the joint inversion has no direct information and the interpolation between distant stations may add spurious structure. Furthermore, this model is more reliable at depths greater than ~200 km where the joint inversion deviates least from the initial model. However, the teleseismic surface wave only model is less reliable in the crust due to the period range of the earthquake data, whereas the joint inversion includes both PRF and ANT derived phase velocities, both of which are primarily sensitive to the crust. As our focus is on the center of Hudson Bay and the lithospheric mantle, we use the *Darbyshire et al*. [2013] model to compare against the SdP CCP model in the following sections, but note that the differences between these two models reflects the nonuniqueness of surface wave inversions.

3.2. Lithospheric Thickness

Determination of the LAB by receiver functions or surface wave inversions alone in cratonic regions is often unclear [e.g., *Eaton et al*., 2009; *Fischer* et al., 2010; *Miller and Eaton*, 2010]. In Phanerozoic regions, the LAB

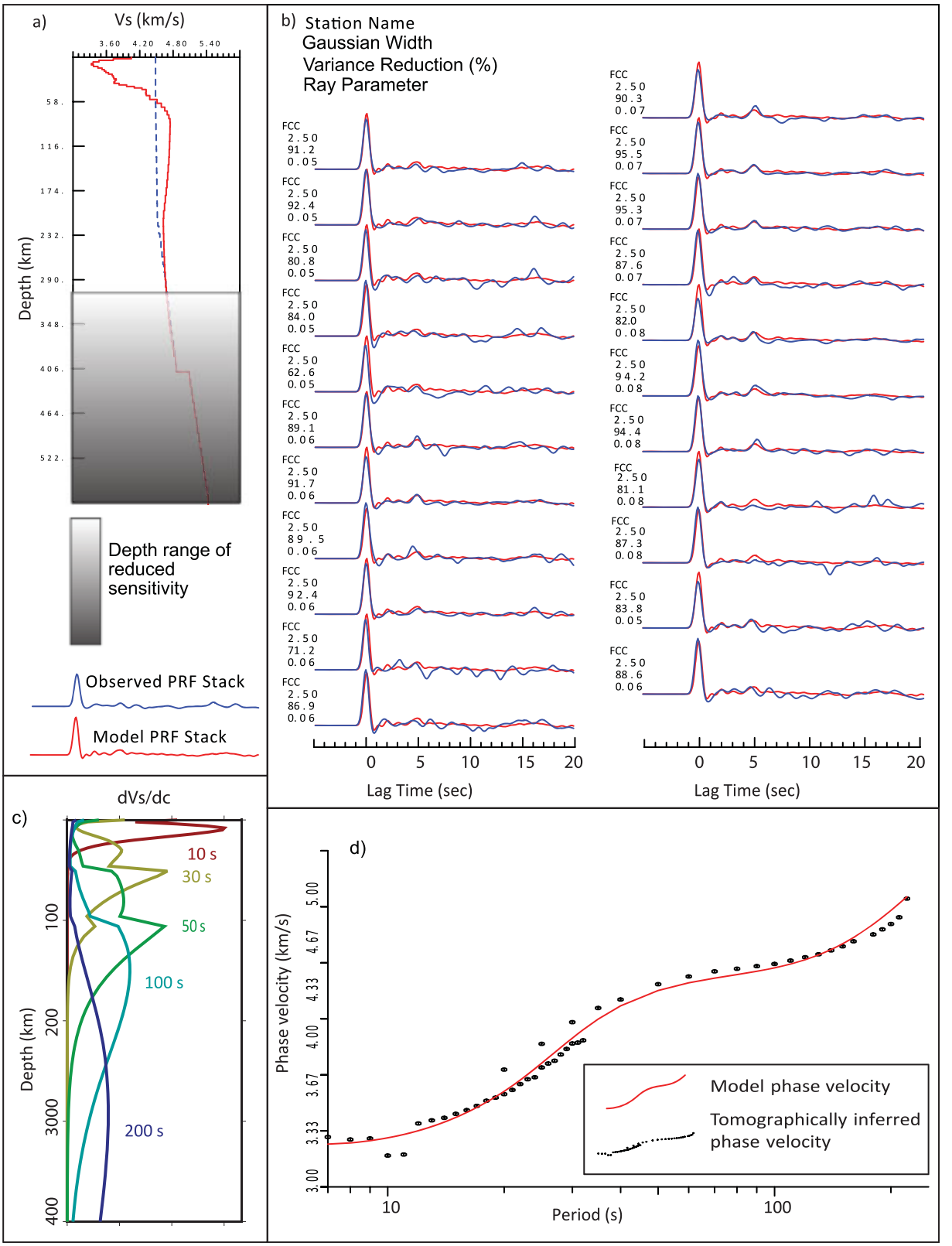

Figure 3. Results of an example joint inversion. (a) Starting model (blue) and final model (red). (b) Stacked PRF and the final model synthetics. (c) Example sensitivity kernels at 10, 30, 50, 100, and 200 s period calculated with a mean shear velocity model for the Hudson Bay region. (d) Fit to the phase velocity data. The low phase velocities at 10 and 12 s are not reliable and thus skipped in the fit. For the model fits at the rest of the stations, see the supporting information.

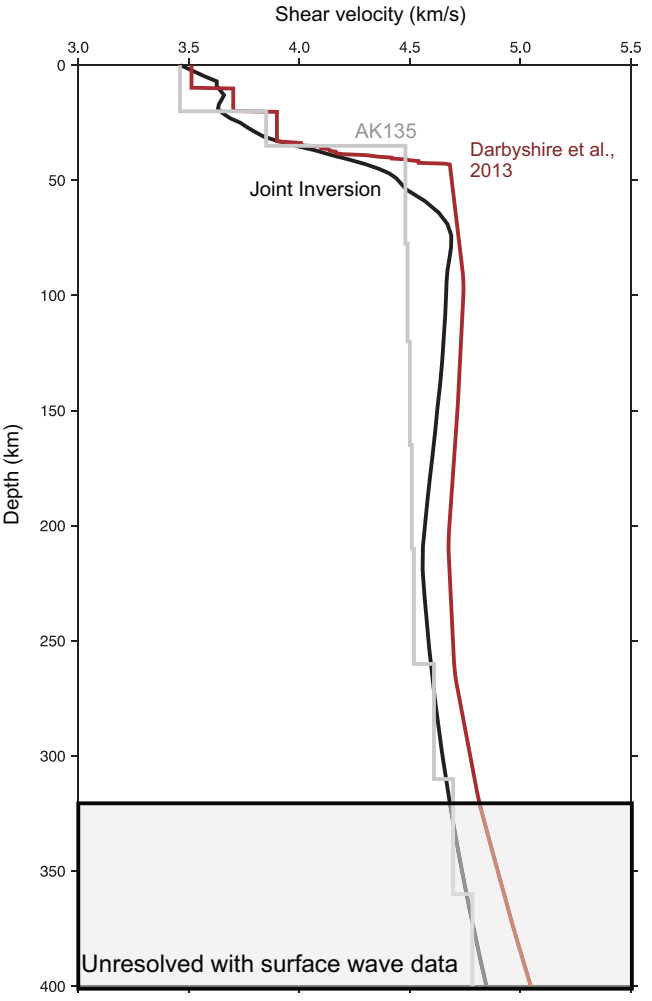

Figure 4. Mean shear velocity curve for Hudson Bay (black), AK135 (gray) [*Kennett et al.*, 1995], and the *Darbyshire et al.* [2013] mean model (dark red).

may be clearly identified with a negative pulse in receiver functions due to a sharp contrast in velocity across the thermal boundary between the conductive lithosphere and convecting asthenosphere. This sharp contrast is not consistently observed in cratonic regions and thus using surface wave proxies has been more common. However, due to the broad surface wave sensitivity kernels at depths greater than ~200 km and their long lateral wavelength, they provide a low-resolution estimate of the LAB depth. In order to make the most reliable LAB estimate for the region, we manually picked an interface through negative conversions in the SdP CCP coincident with the 1.7% fast contour of the shear velocity results of *Darbyshire et al.* [2013] (Figure 6). The picking is done through a series of west to east cross sections and then repeated along a series of south to north cross sections through the CCP volume. The points with an LAB pick are shown in Figure 6a, and Figures 6b and 6c show an example west to east cross section with the LAB picks. The picks are then interpolated to form a smooth surface (Figure 7), which is able to transition between contiguous horizontal layers to account for the poor sensitivity of receiver functions to dipping structures. This method of interpretation indicates that the thickest lithosphere is located under the center of Hudson Bay, coincident with a high amplitude negative conversion.

3.3. Discontinuity Structure

Cross-section views of the discontinuity structure and their associated hit counts are shown in Figures 8 and 9. All cross sections show a positive conversion associated with the Moho at locations along the profile where the hit count indicates nonzero sampling. Section B-B′ (Figure 8c), shows two clear negative conversions; one is at ~80–160 km depth and the other is at ~350 km depth, which we interpret as the LAB. This deep conversion through the center of Hudson Bay is of higher amplitude and more continuous than the LAB conversions north and south of the Bay. The southernmost section, C-C′, shows a shallower lithosphere (~240 km) above a deeper negative (~350 km) near the Great Meteor Hotspot track [*Heaman and Kjarsgaard*, 2000; *Eaton and Frederiksen*, 2007; *Frederiksen et al.*, 2007]. The north to south sections (Figure 9) depict the thick lithosphere under the Bay, thinning in the northern Rae and southern Superior, and shallow (~80 km deep) negative conversions in sections X-X′ and Y-Y′, while section Z-Z′ shows more variable structure. The most notable structures in these north to south profiles are the shallow negative conversions at ~80–100 km depth in X-X′ and Y-Y′. The furthest west section X-X′, crosses through the Rae, Hearne, and Superior, and shows the highest amplitude negative conversion is in the Superior. The amplitude reduces to the north where the LAB shallows between the Rae and Hearne. Y-Y′ shows two more isolated negative conversions, one to the north and one to the south of the center of the profile, however the sampling in

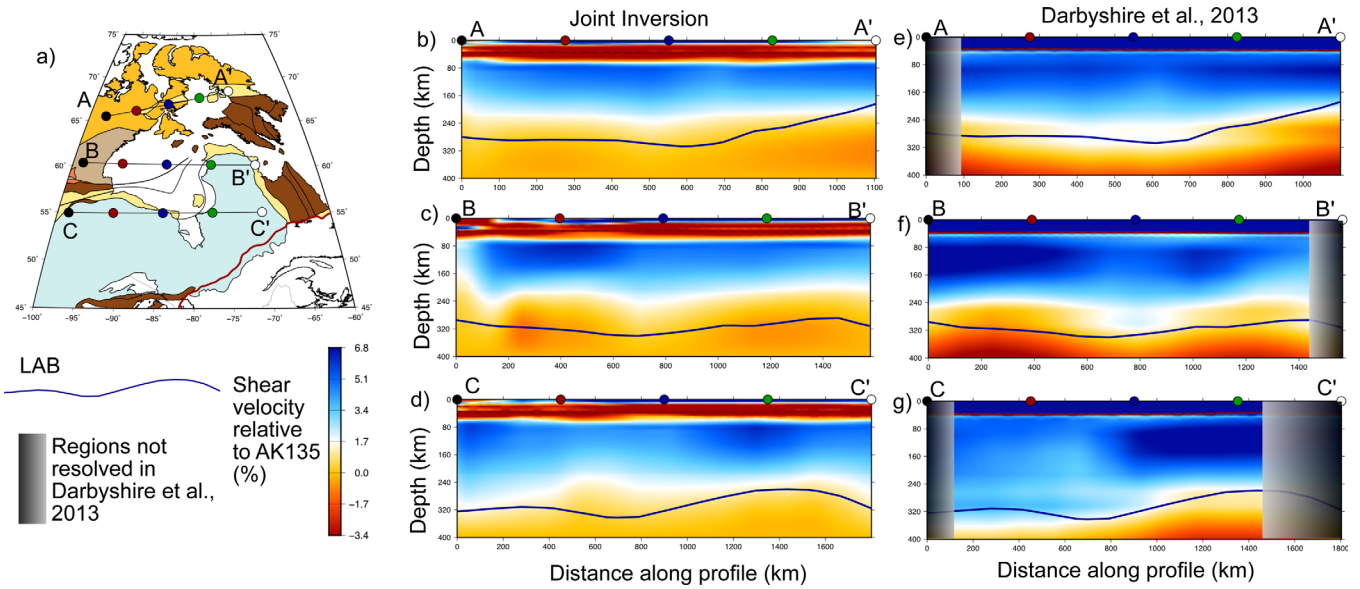

Figure 5. (b–d) Comparison of shear velocity between the joint inversion model and the model of *Darbyshire et al.* [2013]. Locations of the profiles are indicated in Figure 5a and the color palette is consistent in all cross sections. Velocities are relative to the global reference model AK135 [*Kennett et al.*, 1995] and regions outside of the coverage of *Darbyshire et al.* [2013] are shaded out. Dark blue line indicates the LAB inferred from this study and plotted in Figure 7.

the shallow central part of the profile is relatively poor and thus we are unable to say whether this is one continuous surface or two independent anomalies.

4. Discussion

4.1. Thick Lithosphere and MLD

The ~350 km thick lithosphere inferred under the center of Hudson Bay is in stark contrast to the surrounding provinces and prior studies such as *Yuan and Romanowicz* [2010] which estimate lithospheric thicknesses of 200–240 km depth from variations in anisotropy or *Darbyshire et al.* [2013] where the maximum lithospheric thickness reaches ~280–300 km based on isotropic shear velocity proxies. Much of the Rae

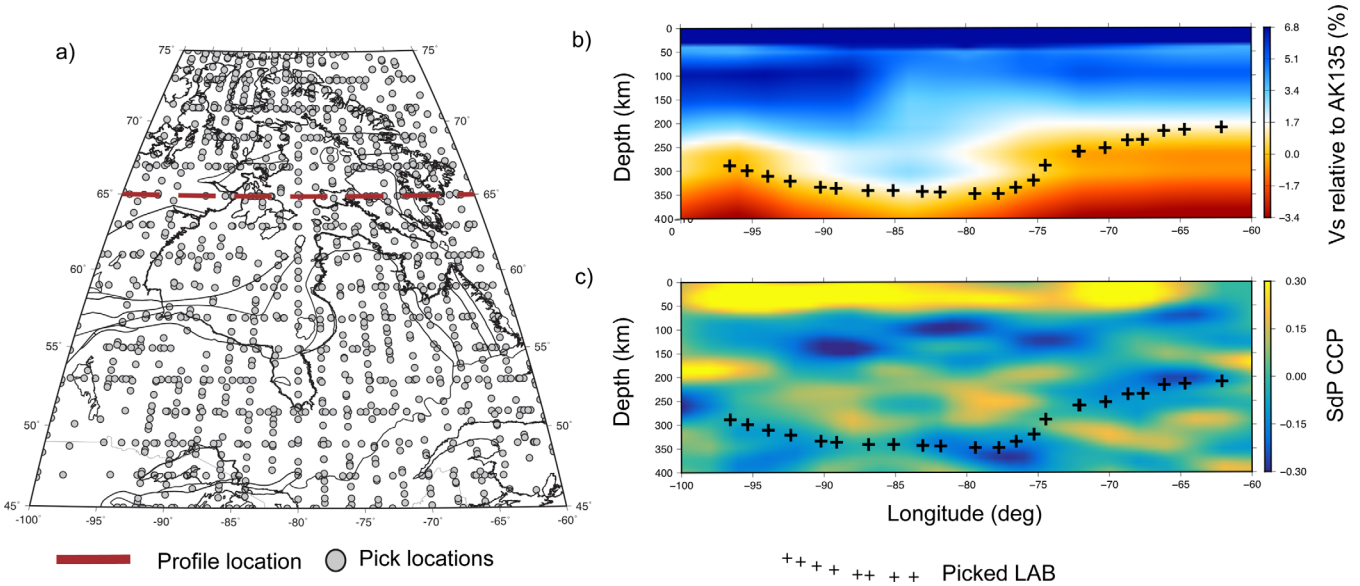

Figure 6. (a) Locations used in estimating the LAB plotted as gray circles. Red line indicates the location of the cross section shown in Figures 6b and 6c. (b) Shear velocity model of *Darbyshire et al.* [2013] with Vs relative to AK135. Black crosses show the picked LAB. (c) SdP CCP image for the same profile as in Figure 6b and the red line in Figure 6a.

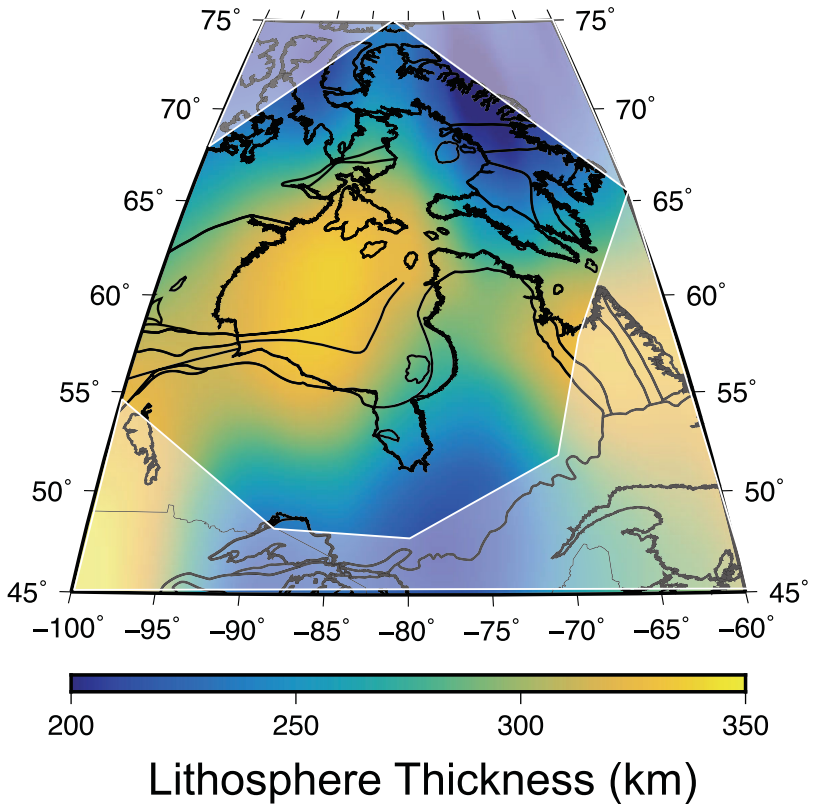

Figure 7. Thickness of the lithosphere from joint interpretation of the SdP CCP volume and the shear velocity model of *Darbyshire et al.* [2013]. Regions with white shading are outside the coverage of *Darbyshire et al.* [2013], but are still covered by the SdP CCP volume.

domain is only ∼240 km thick, while parts of the Hearne reach ∼300 km thickness (Figure 10). Further to the south-east, the Superior-Grenville LAB is a prominent negative conversion at ∼200 km, but the western Superior craton appears to reach 250–300 km thick and the central Superior appears relatively thinned above the Great Meteor Hotspot track (∼200 km). While it has been observed before that the center of the Bay has the thickest lithosphere [*Darbyshire et al.*, 2013], it remains unexpected as this lithosphere was

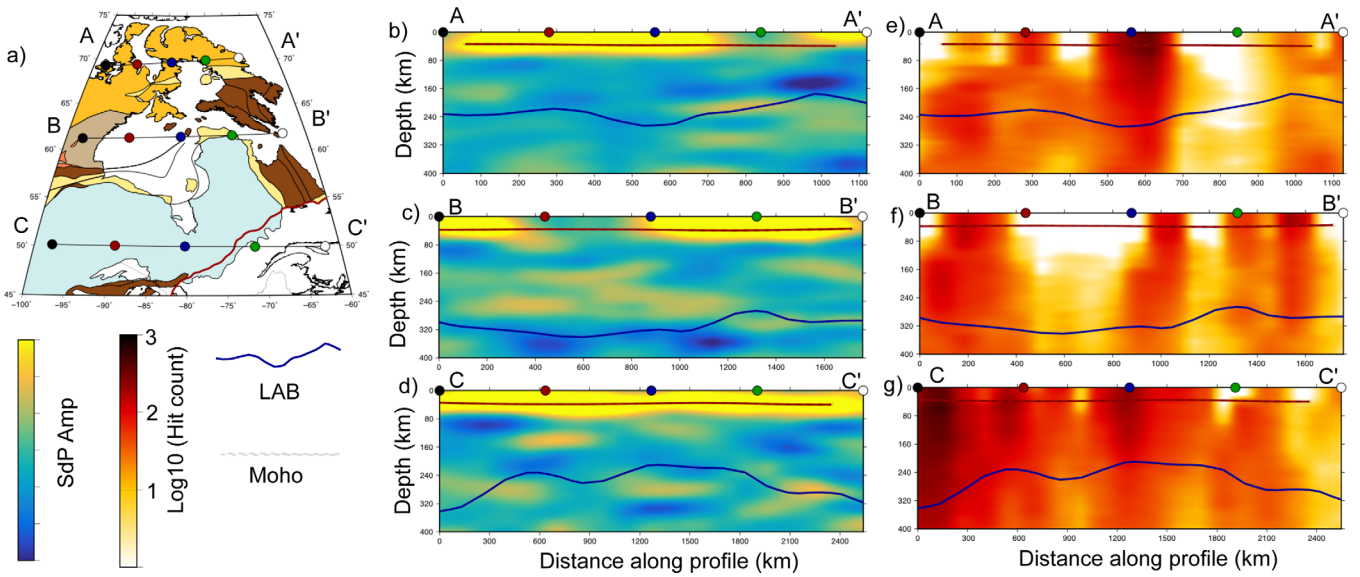

Figure 8. West-east cross sections of (b–d) SdP CCP amplitude and(e–g) log10 hit count. Profile locations indicated in Figure 8a. Dark blue line is the LAB shown in map view in Figure 7.

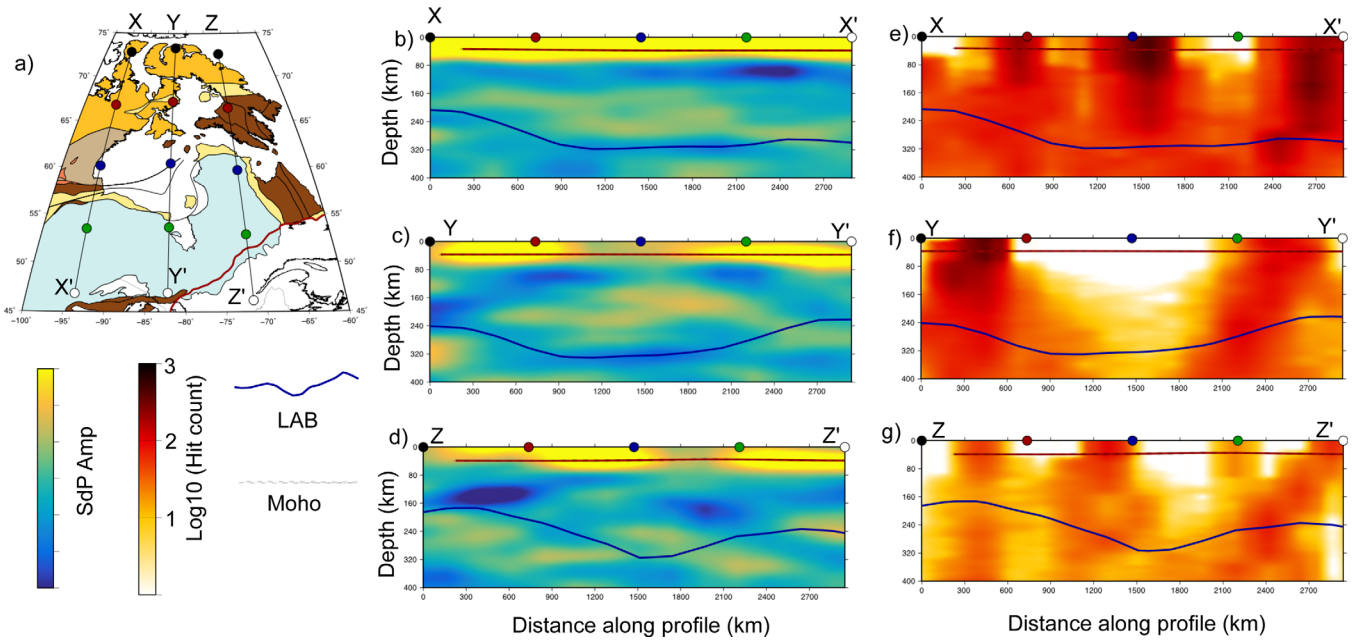

Figure 9. North-south cross sections of (b–d) SdP CCP amplitude and (e–g) log10 hit count. Profile locations indicated in Figure 9a. Dark blue line is the LAB shown in map view in Figure 7.

formed during the closure of an ocean basin during the Trans-Hudson Orogen, rather than during initial formation of the Western Churchill or Superior cratons. Therefore, the observed thickness implies a few possibilities. First, captured ocean arc terranes may have deformed plastically and extended in the vertical dimension in response to lateral squeezing of ocean closure. Second, the center of the Bay may have localized subduction processes leading to focused arc differentiation or stacking of slabs. Thirdly, secular cooling may have been most prevalent in the center of the Bay as it was insulated from mantle circulation since the THO. Finally, the center of the Bay may have down-warped under either its negative thermal buoyancy or due to a downward pull force as slabs subducted beneath it, but remained neutrally buoyant due to its internal strength and positive compositional buoyancy.

The first two mechanisms follow from a primarily plate tectonic model during the Paleoproterozoic. Terrane capture within Hudson Bay has been shown from potential field modeling [*Eaton and Darbyshire*, 2010] making the hypothesis of thickening through compression of these terranes appealing. However, we would need more information on the mass balance and deformation mechanisms to support this hypothesis. Notably, it is not yet clear how the captured terranes would vertically thicken, and produce low density, high seismic velocity material to ~350 km depth. The second mechanism, stacking of oceanic plates or accumulation of arc magmas, is also unviable because this would argue for 1.8–1.9 Ga age subduction-derived products appearing around the peripheries (i.e., in the Rae domain, Hearne domain, or Superior craton), which would have acted as the back arcs during closure. Barring large-scale subduction polarity reversals, we argue that this mechanism does not account for the thickened lithosphere under Hudson Bay.

The secular cooling of the lithosphere over geologic time may contribute significantly to the observed lithospheric thickness. Hudson Bay represents the center of the modern craton, but this formed in the Proterozoic and the surrounding Western Churchill and Superior cratons formed in the Archean. Thus the reverse would be expected: the older Superior and Western Churchill should have had more time to cool and form thick lithosphere. However, cooling models by *Eaton and Perry* [2013] suggest stable buoyancy of cratons forms by ~1 Gyr regardless of whether the craton formed by slab stacking or plume extraction. Therefore, however the core of the craton formed, the internal thermal structure should be equilibrated since the ~1.8 Ga THO.

The last mechanism follows the geodynamic modeling work of *Cooper and Miller* [2014]. This model suggests that craton formation occurs by thickening of material over a mantle downwelling. This produces a locally thickened lithosphere over the downwelling and generates zones of localized deformation around

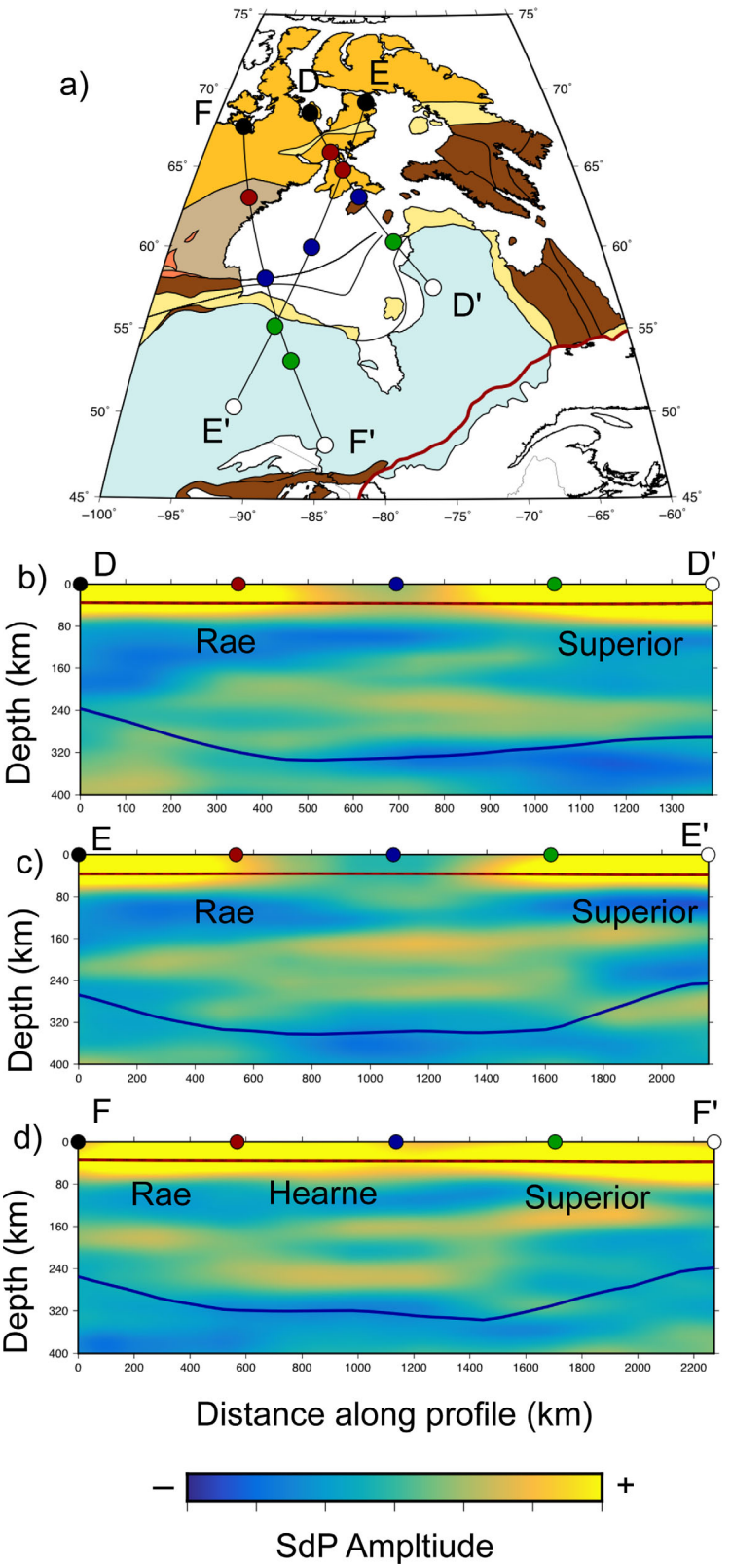

Figure 10. Cross sections traversing Hudson Bay. (a) Locations of the profiles. (b) Profile from the Rae domain to the eastern Superior province. This is the same profile as analyzed in *Snyder et al.* [2013]. (c) Profile from the eastern Rae to the western Superior. (d) Profile from the western Rae through the Hearne to the central Superior. The dark blue line is the inferred LAB as shown in map view in Figure 7.

the periphery. These deformation zones are observed in the form of MLDs around the cratons [*Cooper and Miller*, 2014]. Our SdP CCP model shows these MLDs throughout the region and most prominently around the periphery of Hudson Bay. Therefore, we infer that after the initial formation of continental lithosphere under Hudson Bay, possibly through lateral tectonic processes, the early continental lithosphere downwarped and formed localized shear zones around the periphery in response to this process in the Proterozoic cratonization phase. However, the SdP CCP volume lacks resolution at MLD depths in the center of Hudson Bay and therefore we cannot assert a lack of an MLD under Hudson Bay without more data. Furthermore, the nature of MLDs is still unclear [e.g., *Selway et al*., 2015] and thus the presence of other structures which may manifest as MLDs cannot be discounted.

The MLDs in the SdP CCP volume show patterns that suggest deformation was localized in shear zones primarily consistent with prior zones of weakness from formation. In Figure 10b, a cross section equivalent to that presented in *Snyder et al*. [2013], we observe negative conversions separately between the Rae and Superior across the northeast promontory of THO collision. The dips of these features are difficult to constrain with SdP imaging, but the clear separation of MLDs across this section is consistent with that shown in the anisotropic receiver function imaging of *Snyder et al*. [2013] and interpreted as shear zones. However, with a fully 3-D model, our SdP CCP imaging indicates that these layers are more pervasive than previously thought. Moreover, in addition to the ~80–100 km deep MLD seen in the Rae and Superior, a deeper (~200 km) discontinuity is seen between the Hearne and Superior as section F-F′ (Figure 10d) crosses the Bay. We suspect this might be related to a trapped terrane as modeled in *Eaton and Darbyshire* [2010] or a deep compositional boundary.

4.2. LAB Amplitude

The high amplitude negative conversion at ~350 km depth beneath central Hudson Bay is unusual for an inferred cratonic LAB [e.g., *Eaton et al*., 2009]. Discussions in *Fischer et al*. [2010] argue that the lack of observable LAB in some cratons may be due to a broad velocity gradient from a purely thermal contrast spread over ~70 km in vertical thickness. *Miller and Eaton* [2010] model this as a broad change in velocity and find it does not create a sharp LAB conversion. However, if they input a sharper velocity contrast, they are able to recover a higher amplitude negative SdP conversion at the LAB. The observation of a high amplitude LAB under Hudson Bay can therefore be inferred to be a relatively sharp velocity contrast. While we cannot rule out a compositional or mechanical change, attributing this contrast to a primarily thermal origin suggests we are observing the thermal insulation effect invoked in the Wilson cycle of supercontinents [e.g., *Grigné and Labrosse*, 2001]. This direct observation of the thermally insulated upper mantle suggests the blanketing effect occurs not only under the supercontinents, but is able to develop as the cratons move apart. Furthermore, because of the relative motion of the lithosphere and asthenosphere, we suggest this effect occurs over time scales of a few tens of millions of years and thus is a relatively recent (Phanerozoic) development compared with the formation of the craton. How widespread this effect is, however, will require comparable studies at other cratons worldwide.

5. Conclusions

We present a new SdP CCP volume for the Hudson Bay region and estimates of shear velocity from the joint inversion of Rayleigh wave phase velocities and PdS receiver functions. The thickest lithosphere observed is directly under Hudson Bay, reaching ~350 km depth and having an unusually large amplitude negative conversion in the SdP receiver functions. This conversion is direct evidence of the blanketing effect of continents on the underlying asthenosphere, which is an important element in the supercontinent cycle. Furthermore, we observe midlithospheric discontinuities at ~80–120 km depth through much of the region, which we interpret to reflect localized deformation as the craton down-warped to its current thickness. More work, however, needs to be done to distinguish whether these deformation zones formed due to the influence of stress through the lithosphere or as formational zones of weakness being reactivated. Nonetheless, combining both shear velocity information and discontinuity information has proven to be more useful than either single observation and provides new insight into the formation of the Archean North American continental lithosphere.

Acknowledgments

We would like to thank the Canadian National Seismic Network, IRIS, and Andrew Frederiksen from University of Manitoba for providing seismic data for this study. This work was greatly improved by editor C-T. Lee and reviews from three anonymous reviewers. Iain Bailey and Leland O'Driscoll assisted in the early stages of this study. All figures made with GMT [*Wessel and Smith*, 2006]. Funding provided by NSF EAR Postdoctoral Fellowship grant 1249776. The three dimensional discontinuity and velocity models are available are the IRIS Earth Model Collaboration website and the author's website https://www.robporritt.wordpress.com/HudsonBay.

References

Abt, D. L., K. M. Fischer, S. W. French, H. A. Ford, H. Yuan, and B. Romanowicz (2010), North American lithospheric discontinuity structure imaged by Ps and Sp receiver functions, *J. Geophys. Res. 115*, B09301, doi:10.1029/2009JB006914.

Aulbach, S. (2012), Craton nucleation and formation of thick lithospheric roots, *Lithos*, *149*, 16–30, doi:10.1016/j.lithos.2012.02.011.
Bailey, I. W., M. S. Miller, K. Liu, and A. Levander (2012), V_S and density structure beneath the Colorado Plateau constrained by gravity anomalies and joint inversions of receiver function and phase velocity data, *J. Geophys. Res.*, *117*, B02313, doi:10.1029/2011JB008522.
Barmin, M. P., M. H. Ritzwoller, and A. L., Levshin (2001), A fast and reliable method for surface wave tomography, *Pure Appl. Geophys.*, *158*(8), 1351–1375.
Bastow, I. D., D. A. Thompson, J. Wookey, J. M. Kendall, G. Helffrich, D. B. Snyder, D. W. Eaton, and F. A. Darbyshire (2011), Precambrian plate tectonics: Seismic evidence from northern Hudson Bay, Canada, *Geology*, *39*(1), 91–94, doi:10.1130/g31396.1.
Bastow, I. D., D. W. Eaton, J. M. Kendall, G. Helffrich, D. B. Snyder, D. A. Thompson, J. Wookey, F. A. Darbyshire, and A. Pawlak (2014), The Hudson Bay Lithospheric Experiment (HuBLE): Insights into Precambrian plate tectonics and the development of mantle keels, *Geol. Soc. Spec. Publ.*, *389*, 41–67, doi:10.1144/SP389.7.
Bensen, G. D., M. H. Ritzwoller, M. P. Barmin, A. L. Levshin, F. Lin, M. P. Moschetti, N. M. Shapiro, and Y. Yang (2007), Processing seismic ambient noise data to obtain reliable broad-band surface wave dispersion measurements, *Geophys. J. Int.*, *169*(3), 1230–1290, doi: 10.1111/j.1365-246X.2007.03374.x.
Cooper, C. M., and M. S. Miller (2014), Craton formation: Internal structure inherited from closing of the early oceans, *Lithosphere*, *6*(1), 35–42.
Dalziel, I. W. D. (1991), Pacific margins of Laurentia and East Antarctica-Australia as a conjugate rift pair: Evidence and implications for an Eocambrian supercontinent, *Geology*, *19*, 598–601, doi:10.1130/0091-7613.
Darbyshire, F. A., and D. W. Eaton (2010), The lithospheric root beneath Hudson Bay, Canada from Rayleigh wave dispersion: No clear seismological distinction between Archean and Proterozoic mantle, *Lithos*, *120*(1-2), 144–159, doi:10.1016/j.lithos.2010.04.010.
Darbyshire, F. A., and S. Lebedev (2009), Rayleigh wave phase-velocity heterogeneity and multilayered azimuthal anisotropy of the Superior Craton, Ontario, *Geophys. J. Int.*, *176*(1), 215–234, doi:10.1111/j.1365-246X.2008.03982.x.
Darbyshire, F. A., D. W. Eaton, A. W. Frederiksen, and L. Ertolahti (2007), New insights into the lithosphere beneath the Superior Province from Rayleigh wave dispersion and receiver function analysis, *Geophys. J. Int.*, *169*(3), 1043–1068, doi:10.1111/j.1365-246X.2006.03259.x.
Darbyshire, F. A., D. W. Eaton, and I. D. Bastow (2013), Seismic imaging of the lithosphere beneath Hudson Bay: Episodic growth of the Laurentian mantle keel, *Earth Planet. Sci. Lett.*, *373*, 179–193, doi:10.1016/j.epsl.2013.05.002.
Davis, W. J., S. Hanmer, and H. A. Sandeman (2004), Temporal evolution of the Neoarchean Central Hearne supracrustal belt: Rapid generation of juvenile crust in a suprasubduction zone setting, *Precambrian Res.*, *134*(1-2), 85–112, doi:10.1016/j.precamres.2004.02.002.
Davis, W. J., S. Hanmer, S. Tella, H. A. Sandeman, and J. J. Ryan (2006), U-Pb geochronology of the MacQuoid supracrustal belt and Cross Bay plutonic complex: Key components of the northwestern Hearne subdomain, western Churchill Province, Nunavut, Canada, *Precambrian Res.*, *145*(1-2), 53–80, doi:10.1016/j.precamres.2005.11.016.
Deschamps, F., S. Lebedev, T. Meier, and J. Trampert (2008), Azimuthal anisotropy of Rayleigh-wave phase velocities in the east-central US, *Geophys. J. Int.*, *173*, 827–843, doi:10.1111/j.1365-246X.2008.03751.x.
Dziewonski, A. M., S. Block, and M. Landisman (1969), A technique for analysis of transient seismic signals, *Bull. Seismol. Soc. Am.*, *59*, 427–444.
Eagar, K. C., and M. J. Fouch (2012), FuncLab: A MATLAB interactive toolbox for handling receiver function datasets, *Seismol. Res. Lett.*, *83*, 596–603, doi:10.1785/gssrl.83.3.596.
Eaton, D. W., and F. Darbyshire (2010), Lithospheric architecture and tectonic evolution of the Hudson Bay region, *Tectonophysics*, *480*(1-4), 1–22, doi:10.1016/j.tecto.2009.09.006.
Eaton, D. W., and A. Frederiksen (2007), Seismic evidence for convection-driven motion of the North American plate, *Nature*, *446*, 428–431, doi:10.1038/nature05675.
Eaton, D. W., and H. K. C. Perry (2013), Ephemeral isopycnicity of cratonic mantle keels, *Nat. Geosci. 6*, 967–970, doi:10.1038/NGEO1950.
Eaton, D. W., F. Darbyshire, R. L. Evans, H. Grütter, A. G. Jones, and X. Yuan (2009), The elusive lithosphere-asthenosphere boundary (LAB) beneath cratons, *Lithos*, *109*, 1–22, doi:10.1016/j.lithos.2008.05.009.
Fischer, K. M., H. A. Ford, D. L. Abt, and C. A. Rychert (2010), The lithosphere-asthenosphere boundary, *Annu. Rev. Earth Planet. Sci.*, *38*, 551–575, doi:10.1146/annurev-earth-040809–152438.
Ford, A. H., K. M. Fischer, D. L. Abt, C. A. Rychert, and L. T. Elkins-Tanton (2010), The lithosphere-asthenosphere boundary and cratonic lithospheric layering beneath Australia from Sp wave imaging, *Earth Planet. Sci. Lett.*, *300*, 299–310. doi:10.1016/j.epsl.2010.10.007.
Foster, K., K. Dueker, B. Schmandt, and H. Yuan (2013), A sharp cratonic lithosphere-asthenosphere boundary beneath the American Midwest and its relation to mantle flow, *Earth Planet. Sci. Lett.*, *402*, 82–89, doi:10.1016/j.epsl.2013.11.018.
Frederiksen, A. W., S. K. Miong, F. A. Darbyshire, D. W. Eaton, S. Rondenay, and S. Sol (2007), Lithospheric variations across the Superior Province, Ontario, Canada: Evidence from tomography and shear wave splitting, *J. Geophys. Res.*, *112*, B07318, doi:10.1029/2006JB004861.
Gibb, R. A. (1983), Model for suturing of Superior and Churchill plates—An example of double indentation tectonics, *Geology*, *11*(7), 413–417, doi:10.1130/0091-7613(1983)11<413:mfsosa>2.0.co;2.
Grigné, C. and S. Labrosse (2001), Effects of continents on Earth cooling: Thermal blanketing and depletion in radioactive elements, *Geophys. Res. Lett. 28*(14), 2707–2710.
Gung, Y. M. Paning, and B. Romanowicz (2003), Global anisotropy and the thickness of continents, *Nature*, *422*, 707–711, doi:10.1038/nature01559.
Hansen, S. M., K. G. Dueker, J. C. Stachnik, R. C. Aster, and K. E. Karlstrom (2013), A rootless rockies—Support and lithospheric structure of the Colorado Rocky Mountains inferred from CREST and TA seismic data, *Geochem. Geophys. Geosyst.*, *14*, 2670–2695, doi:10.1002/ggge.20143.
Heaman, L., and B. Kjarsgaard (2000), Timing of eastern North American kimberlite magmatism: Continental extension of the Great Meteor hotspot track?, *Earth Planet. Sci. Lett.*, *178*, 253–268.
Herrmann, R. B. (2013), Computer programs in seismology: An evolving tool for instruction and research, *Seismol. Res. Lett.*, *84*(6), 1081–1088, doi:10.1785/0220110096.
Jaupart, C., and J. C. Mareschal (1999), The thermal structure and thickness of continental roots, *Lithos*, *48*, 93–114.
Jordan, T. H. (1988), Structure and formation of the continental tectosphere, *J. Petrol.*, *1*, 11–37, doi:10.1093/petrology/Special_Volume.1.11.
Julia, J., C. J. Ammon, R. B. Herrmann, and A. M. Correig (2000), Joint inversion of receiver function and surface wave dispersion observations, *Geophys. J. Int.*, *143*(1), 99–112, doi:10.1046/j.1365-246x.2000.00217.x.
Kennett, B. L. N., E. R. Engdahl, and R. Buland (1995), Constraints on seismic velocities in the Earth from traveltimes, *Geophys. J. Int.*, *122*(1), 108–124, doi:10.1111/j.1365-246X.1995.tb03540.x.

Kind, R., X. Yuan, and P. Kumar (2012), Seismic receiver functions and the lithosphere-asthenosphere boundary, *Tectonophysics*, *536*, 25–43, doi:10.1016/j.tecto.2012.03.005.
Kumar, P., R. Kind, X. Yuan, and J. Mechie (2012), USArray Receiver Function Images of the Lithosphere-Asthenosphere Boundary, *Seismol. Res. Lett.*, *83*(3), 486–491, doi:10.1785/gssrl.83.3.486.
Langston, C. A. (1977), Corvallis, Oregon, crustal and upper mantle receiver structure from teleseismic P-waves and S-waves, *Bull. Seismol. Soc. Am.*, *67*(3), 713–724.
Lee, C.-T. A. (2006), Geochemical/petrologic constraints on the origin of cratonic mantle, in *Archean Geodynamics and Environments*, edited by K. Benn, J.-C. Mareschal, and K. C. Condie, AGU, Washington, D. C., doi:10.1029/164GM08.
Lekic, V., and B. Romanowicz (2011), Inferring upper-mantle structure by full waveform tomography with the spectral element method, *Geophys. J. Int.*, *185*(2), 799–831, doi:10.1111/j.1365-246X.2011.04969.x.
Lekic, V., S. W. French, and K. M. Fischer (2011), Lithospheric thinning beneath rifted regions of Southern California, *Science*, *334*(6057), 783–787, doi:10.1126/science.1208898.
Lenardic, A., L.-N. Moresi, A. M. Jellinek, and M. Manga (2005), Continental insulation, mantle cooling, and the surface area of oceans and continents, *Earth Planet. Sci. Lett.*, *234*, 317–333, doi:10.1016/j.epsl.2005.01.038.
Levander, A., and M. S. Miller (2012), Evolutionary aspects of lithosphere discontinuity structure in the western US, *Geochem. Geophys. Geosyst.*, *13*, Q0AK07, doi:10.1029/2012GC004056.
Levshin, A. L., T. B. Yanovskaia, A. V. Lander, B. G. Bukchin, M. P. Barmin, L. I. Ramikova (1989), Surface waves in vertically inhomogeneous media, in *Surface Waves in a Laterally Inhomogeneous Earth*, in edited by V. I. Keilis-Borok, pp. 131–182, Kluwer Acad. Publ., Dordrecht, Netherlands.
Lévy, F., C. Jaupart, J.-C. Mareschal, G. Bienfait, and A. Limare (2010), Low heat flux and large variations of lithospheric thickness in the Canadian Shield, *J. Geophys. Res.*, *115*, B06404, doi:10.1029/2009JB006470.
Ligorria, J. P., and C. J. Ammon (1999), Iterative deconvolution and receiver-function estimation, *Bull. Seismol. Soc. Am.*, *89*(5), 1395–1400.
Liu, K. J., A. Levander, Y. B. Zhai, R. W. Porritt, and R. M. Allen (2012), Asthenospheric flow and lithospheric evolution near the Mendocino Triple Junction, *Earth Planet. Sci. Lett.*, *323*, 60–71, doi:10.1016/j.epsl.2012.01.020.
Miller, M. S., and N. P. Agostinetti (2011), Erosion of the continental lithosphere at the cusps of the Calabrian arc: Evidence from S receiver functions analysis, *Geophys. Res. Lett.*, *38*, L23301, doi:10.1029/2011GL049455.
Miller, M. S., and N. P. Agostinetti (2012), Insights into the evolution of the Italian lithospheric structure from S receiver function analysis, *Earth Planet. Sci. Lett.*, *345*, 49–59, doi:10.1016/j.epsl.2012.06.028.
Miller, M. S., and D. W. Eaton (2010), Formation of cratonic mantle keels by arc accretion: Evidence from S receiver functions, *Geophys. Res. Lett.*, *37*, L18305, doi:10.1029/2010GL044366.
Moores, E. M. (1991), The Southwest U.S.-East Antarctica (SWEAT) connection: A hypothesis, *Geology*, *19*, 425–428, doi:10.1130/0091–7613.
O'Driscoll, L. J., and M. S. Miller (2015), Lithospheric discontinuity structure in Alaska, thickness variations determined by Sp receiver functions, *Tectonics*, *34*, 694–714, doi:10.1002/2014TC003669.
Pawlak, A., D. W. Eaton, I. D. Bastow, J. M. Kendall, G. Helffrich, J. Wookey, and D. Snyder (2011), Crustal structure beneath Hudson Bay from ambient-noise tomography: Implications for basin formation, *Geophys. J. Int.*, *184*(1), 65–82, doi:10.1111/j.1365-246X.2010.04828.x.
Pawlak, A., D. W. Eaton, F. Darbyshire, S. Lebedev, and I. D. Bastow (2012), Crustal anisotropy beneath Hudson Bay from ambient noise tomography: Evidence for post-orogenic lower-crustal flow?, *J. Geophys. Res.*, *117*, B08301, doi:10.1029/2011JB009066.
Percival, J. A. (2007), Geology and metallogeny of the Superior Province, Canada, in *Mineral Deposits of Canada: A Synthesis of Major Deposit-Types, District Metallogeny, the Evolution of Geological Provinces, and Exploration Methods*, in edited by W. D. Goodfellow, pp. 903–928, Geological Association of Canada, Mineral Deposits Division, Toronto, Ontario, Canada.
Peterson, T. D., S. Phersson, T. Skulski, and H. Sandeman (2011), Compilation of Sm-Nd isotope analyses of igneous suites, western Churchill Province, *Geol. Surv. Can. Open File*, *6439*, 18.
Pollack, H. N., S. J. Hurter, and J. R. Johnson (1993), Heat flow from the Earth's interior: Analysis of the global data set, *Rev. Geophys.*, *31*(3), 267–280.
Rolandone, F., J.-C. Mareschal, C. Jaupart, C. Gosselin, G. Bienfait, and R. Lapointe (2003), Heat flow in the western Superior Province of the Canadian shield, *Geophys. Res. Lett.*, *30*(12), 1637, doi:10.1029/2003GL017386.
Selway, K., H. Ford, and P. Kelemen (2015). The seismic mid-lithosperic discontinuity, *Earth Planet Sci. Lett.*, *414*, 45–57, doi:10.1016/j.epsl.2014.12.029.
Snyder, D. B., R. G. Berman, J. M. Kendall, and M. Sanborn-Barrie (2013), Seismic anisotropy and mantle structure of the Rae craton, central Canada, from joint interpretation of SKS splitting and receiver functions, *Precambrian Res.*, *232*, 189–208, doi:10.1016/j.precamres.2012.03.003.
Thompson, D. A., I. D. Bastow, G. Helffrich, J. M. Kendall, J. Wookey, D. B. Snyder, and D. W. Eaton (2010), Precambrian crustal evolution: Seismic constraints from the Canadian Shield, *Earth Planet. Sci. Lett.*, *297*(3-4), 655–666, doi:10.1016/j.epsl.2010.07.021.
Thompson, D. A., G. Helffrich, I. D. Bastow, J. M. Kendall, J. Wookey, D. W. Eaton, and D. B. Snyder (2011), Implications of a simple mantle transition zone beneath cratonic North America, *Earth Planet. Sci. Lett.*, *312*(1-2), 28–36, doi:10.1016/j.epsl.2011.09.037.
Vinnik, L. P. (1977), Detection of waves converted from P to SV in mantle, *Phys. Earth Planet. Inter.*, *15*(1), 39–45, doi:10.1016/0031-9201(77)90008-5.
Wessel, P., and W. H. F. Smith (2006), New, improved version of generic mapping tools released, *Eos Trans. AGU*, *79*(47), 579, doi:10.1029/98EO00426.
Whitmeyer, S. J., and K. E. Karlstrom (2007), Tectonic model for the Proterozoic growth of North America, *Geosphere*, *3*(4), 220–259, doi:10.1130/ges00055.1.
Yuan, H., and B. Romanowicz (2010), Lithospheric layering in the North American craton, *Nature*, *466*(7310), 1063–1068, doi:10.1038/nature09332.
Yuan, X. H., R. Kind, X. Q. Li, and R. J. Wang (2006), The S receiver functions: Synthetics and data example, *Geophys. J. Int.*, *165* (2), 555–564, doi:10.1111/j.1365-246X.2006.02885.x.